ORIGINAL PAPER

Theoretical models for prediction of mechanical behaviour of the PP/EPDM nanocomposites fabricated by friction stir process

Amir Mostafapour[1], Ghasem Naderi[2], Mohammad Reza Nakhaei[1*]

[1] Faculty of Mechanical Engineering, University of Tabriz, Tabriz, Iran
[2] Faculty of Polymer Processing, Iran Polymer and Petrochemical Institute (IPPI), Tehran, Iran

ABSTRACT

In this study, thermoplastic polyolefin elastomeric (TPO) nanocomposites were fabricated by friction stir processing. The effect of different pin geometries on clay dispersion and mechanical properties of the TPO nanocomposite reinforced with 3% wt nanoclay has been first investigated. The optimum pin geometry namely threaded cylindrical pin was then used to fabricate the nanocomposites containing 3, 5 and 7 wt% nanoclay. The results showed that increase in the clay content increased the tensile strength and tensile modulus of the nanocomposite from 15.8 to 22.76 MPa and 568 to 751 MPa, respectively. The experimental stress – strain curves of nanocomposites were compared with eight constitutive models including Mooney – Rivlin, the second-order polynomial, Neo – Hookean, Yeoh, Arruda – Boyce, Van der Waals and the third- and sixth-order Ogden. The comparisons showed that there was an agreement between the experimental data and the sixth-order Ogden model. Three micromechanical models Halpin – Tsai, inverse rule of mixture and linear rule of mixture were applied to investigate the Young's modulus of nanocomposites. Because of the significant difference between the Young's modulus obtained from these models and the ones obtained from experimental data, a modifying factor was used to improve the theoretical predictions obtained from the models. **Polyolefins J (2017) 4: 99-109**

Keywords: geometry; friction stir process; nanocomposite; clay; mechanical behavior.

INTRODUCTION

Thermoplastic polyolefin elastomeric materials (TPOs) are an important class of polymer blends having a combination of thermoplastic and rubbery properties such as flowability at high temperatures, elastic properties at room temperature and ease of production [1, 2]. Blending thermoplastics like polypropylene (PP) with rubbers like ethylene-propylene diene monomer (EPDM) leads to materials with better toughness and lower stiffness and hardness [3]. The addition of clay at very low proportion enhances mechanical, thermal and barrier properties dramatically [4, 5]. TPO nanocomposites are widely used in many fields such as airplane, automotive, ship parts and medical apparatus [1, 6].

There are different processes to fabricate nanocomposites including solvent blending, in-situ polymerization and melt compounding [7-9]. Recently, investigations have been done on friction stir

Theoretical models for prediction of mechanical behaviour of the PP/EPDM nanocomposites fabricated by friction stir process

IPPI

processing (FSP) for the fabrication of composites and nanocomposites [10-13]. In FSP, the frictional heat softens the polymer matrix and the nanoparticles are dispersed in the processed zone by the stirring action of the tool [14, 15]. According to literatures, very few reports are presented about fabricating polymeric composites and nanocomposites by FSP. For instance, enhancement of morphology and mechanical properties of polyethylene (PE)/copper composite and high density polyethylene (HDPE)/ clay nanocomposite using FSP have been reported by Azarsa et al., and Barmous et al., respectively [16-18]. In this study, the feasibility of fabricating clay containing PP/EPDM nanocomposites using FSP is experimentally investigated. The effect of nanoclay content on the applicability of eight constitutive models to predict stress – strain behavior of the nanocomposites is studied. Finally, based on the experimental data, a modified model is obtained to predict the Yong's modulus of the nanocomposites.

THEORETICAL CONCEPT
Hyperelastic models
Strain energy density (stored energy per unit volume) in a hyperelastic material can be described by the stress – strain behavior. Strain energy function based on three invariants of the strain tensor (I1, I2, I3) is defined as Eq. 1:

$$W = f(I_1, I_2, I_3) = \sum_{i+j+k=1}^{\infty} c_{ijk}(I_1 - 3)^i \times (I_2 - 3)^j \times (I_3 - 1)^k \qquad (1)$$

In which W is the strain energy density (SED) and I_1, I_2 and I_3 are invariants of strain tensor given by:

$$\begin{cases} I_1 = \lambda_1^2 + \lambda_2^2 + \lambda_3^2 \\ I_2 = \lambda_1^2\lambda_2^2 + \lambda_2^2\lambda_3^2 + \lambda_3^2\lambda_1^2 \\ I_3 = \lambda_1^2\lambda_2^2\lambda_3^2 \end{cases} \qquad (2)$$

Where λ_1, λ_2 and λ_3 are three principal stretch ratios. In an incompressible material ($\lambda_1\lambda_2\lambda_3=1$), ($\lambda_1=\lambda$) and $\lambda_2 = \lambda_3 = \lambda^{\frac{-1}{2}}$, therefore $I_3=1$ and Eq. 1 decreases to:

$$W = \sum_{i+j=1}^{\infty} C_{ij}(I_1 - 3)^i \times (I_2 - 3)^j \qquad (3)$$

In this study, eight hyperelastic models are used to

investigate the nonlinear stress – strain behavior of PP/EPDM/clay nanocomposite samples [19-21].

Arruda – Boyce model
The Arruda – Boyce model is based on molecular considerations to explain the stress – strain behavior of rubbers and other polymeric materials. This model calculates the strain energy as the sum of the strain energies of individual chains:

$$W = \mu \sum_{i=1}^{5} \frac{C_i}{\lambda_m^{2i-2}} \times (I_1^i - 3^i) + \frac{1}{D}[\frac{J_{el}^2 - 1}{2} - Ln(J_{el})] \qquad (4)$$

In which C is are material constants where $C_1 = \frac{1}{2}$, $C_2 = \frac{1}{20}$, $C_3 = \frac{11}{1052}$, $C_4 = \frac{19}{7000}$, $C_5 = \frac{519}{673750}$ and J_{el} is the elastic volume ratio. Arruda – Boyce model includes two parameters μ and λ_m, which μ is the initial shear modulus and λ_m is the stretch at which the polymer chain network becomes locked and stress – strain curve rises significantly. μ and λ_m are dependent to the elastomer microstructure. D is equal to 2/k, K is the bulk modulus at small strain, which for an incompressible material is set to zero.

Polynomial Model
The strain energy density potential of polynomial model is expressed based on the 1st and 2nd invariants of strain tensor, I_1 and I_2 as below:

$$W = \sum_{i=0}^{n} \sum_{j=0}^{m} C_{ij} \times (I_1 - 3)^i \times (I_2 - 3)^i + \sum_{i=1}^{n} \frac{1}{D_i}(J_{el} - 1)^{2i} \qquad (5)$$

In which Cijs are material constant describing shear behaviors of the polymer material. When m = n = 2, the second-order polynomial is as below:

$$(6)$$

$$W = C_{10}(I_1 - 3) + C_{01}(I_2 - 3) + C_{11}(I_1 - 3)(I_2 - 3) + C_{20}(I_1 - 3)^2 + C_{02}(I_2 - 3)^2$$

Reduced Polynomial Model
The reduced polynomial model is similar to polynomial form but it is based on the first invariants of strain tensor only. Thus strain energy density becomes:

$$W = \sum_{i=0}^{N} C_{i0} \times (I_1 - 3)^i + \sum_{i=1}^{N} \frac{1}{D_i}(J_{el} - 1)^{2i} \qquad (7)$$

Yeoh model
Yeoh's strain energy density function is a special form of reduced polynomial in which N=3 and is given as below:

$$(8)$$

$$W = C_{10}(I_1 - 3) + C_{01}(I_2 - 3) + C_{11}(I_1 - 3)(I_2 - 3) + C_{20}(I_1 - 3)^2 + C_{02}(I_2 - 3)^2$$

This model is suggested to describe hyperelastic

behavior of rubber parts with extensive deformation under uniaxial tension test.

Neo – Hookean

This model is based on reduced polynomial model when considering N=1 and is introduced as:

$$W = C_{10}(I_1 - 3) \tag{9}$$

Van der Waals model

The Van der Waals model also known as Kialin model describes the strain energy density function as given by:

$$\tag{10}$$

$$W = \mu\left\{-(\lambda_m^2 - 3)[\ln(1-\eta) + \eta] - \frac{2}{3}a\left(\frac{I-3}{2}\right)^{\frac{3}{2}}\right\} + \frac{1}{D}\left[\frac{J_{el}^2 - 1}{2} - \ln(J_{el})\right]$$

In which $I = (1-\beta) I_1 + \beta I_2$ and $\eta = \sqrt{\frac{I-3}{\lambda_m^2 - 3}}$. β, η and a are the invariant mixture parameter, initial shear modulus and global interaction parameter, respectively.

Ogden model

This model can describe hyperelastic behavior of materials assuming $\lambda_1 \lambda_2 \lambda_3 = 1$ through following equation:

$$W = \sum_{i=1}^{N} \frac{2\mu_i}{\alpha_i^2}(\lambda_1^{\alpha i} + \lambda_2^{\alpha i} + \lambda_3^{\alpha i} - 3) + \sum_{i=1}^{N} \frac{1}{D_i}(J_{el} - 1)^{2i} \tag{11}$$

Where μ_i and αi are material constants which explain shear. In this work, strain energy density potentials with N=3 and 6 employed.

Mooney – Rivlin model

The strain energy density function of Mooney - Rivlin model is the special form of Ogden and polynomial models by assuming N=2, $\alpha_1 = 1$ for Ogden and m = n = 1 for polynomial function as below:

$$W = C_{10}(I_1 - 3) + C_{01}(I_2 - 3) \tag{12}$$

Marlow model

The strain energy density function of Marlow model is only a function of the 1st invariant of strain tensor without any explicit relation. The equation for uniaxial strain by the Marlow model can be written as follows:

$$W = \int_0^{\lambda(I_1)-1} \sigma(\varepsilon)d(\varepsilon) \tag{13}$$

In an incompressible material the first invariant of strain tensor can be written as:

$$I_1 = \lambda_1^2 + \lambda_2^2 + \frac{1}{\lambda_1^2 \lambda_2^2} \tag{14}$$

The minimum and maximum values of the I_1 are between 3 and +∞, respectively. In the uniaxial form, λ_1 is equal to $\frac{1}{\lambda_2^{0.5}}$ and I_1 can be written as:

$$I_1 = \lambda^2 - \frac{2}{\lambda} \tag{15}$$

In Eq. 11, σ and ε are the nominal stress and strain that are obtained from experimental uniaxial test, respectively.

Halpin – Tsai Theory

The Halpin – Tsai (H-T) model is the other form of Hill's self-consistent theory which is used to predict the Young's modulus of composites and nanocomposites reinforced with various types of filler [22]. For fully aligned-composite and nanocomposites, Young's modulus can be expressed as:

$$E_{c_{(Halpin-Tsai)}} = E_m\left(\frac{1 + \lambda\eta\varphi_f}{1 - \eta\varphi_f}\right) \tag{17}$$

In which

$$\eta = \frac{\frac{E_f}{E_m} - 1}{\frac{E_f}{E_m} + \lambda} \tag{18}$$

φ_f is the volume fraction of the reinforcing filler and λ is the shape parameter depending on filler geometry, aspect ratio, orientation and loading direction. E is the elastic modulus and the subscripts c, f and m refer to composite, filler and matrix, respectively [23]. H-T equation for a randomly oriented compound is the summation of perpendicular (transverse) and parallel (longitudinal) modulus to the major axis of the fillers as given below:

$$\frac{E_{c_{(Halpin-Tsai)}}}{E_m} = a_L\left(\frac{1 + \lambda_L\eta_L\varphi_f}{1 - \eta_L\varphi_f}\right) + a_T\left(\frac{1 + \lambda_T\eta_T\varphi_f}{1 - \eta_T\varphi_f}\right) \tag{19}$$

Where $a_L = \frac{3}{8}$, $a_T = \frac{5}{8}$, $\lambda_T = 2$ and $\lambda_L = 2\frac{l}{d}$.
In the Halpin - Tsai equation, the shape parameter, λ,

is between 0 and +∞. If λ=+∞ then Eq.14 is reduced to the linear rule of mixtures (LROM) as given below:

$$E_{c_{(LROM)}} = E_f \varphi_f + E_m (1 - \varphi_f) \qquad (20)$$

However, for λ= 0, H-T equation becomes the inverse rule of mixture (IROM) as given below:

$$E_{c_{(LROM)}} = \left(\frac{\varphi_f}{E_f} + \frac{(1 - \varphi_f)}{E_m} \right)^{-1} \qquad (21)$$

EXPERIMENTAL

Material

The TPO matrix and filler used in this work were PP/EPDM blend and nanoclay, respectively. The grade name, company and characterizations of PP, EPDM and nanoclay are shown in Table 1. The blending of TPO composite with 80% wt PP and 20% wt EPDM was carried out in a Brabender co-rotating twin-screw extruder (L/D = 40 and D = 25 mm) with a feeding rate of 0.5 kg/h, a screw speed of 100 rpm and a temperature profile of 185- 200°C and 190°C from the feeding zone to the die. TPO sheets with 200×60×10 mm dimension were prepared using Collin P 200 E-type heat press.

Friction stir processing tool

The FSP tool and fixture used in this study are shown in Figure 1. The FSP tool consists of a heating system, pin and shoulder. Four different tool pin profiles (threaded taper, threaded and straight cylindrical and square) have been used to fabricate the TPO nanocomposite. The geometry and dimensions of threaded pins are shown in Table 2. The pin and shoulder materials were AISI H13 hot-working steel and AA7075 aluminum alloy, respectively. Shoulder's surface was coated with Teflon (PTFE) to prevent sticking of aluminum to the base material surface. An electric heater was used for controlling the temperature of the shoulder and a

Figure 1. Fixture installed on the milling machine.

thermocouple was inserted in a place in the front and at the bottom surface of the shoulder to adjust the heat output of the electric heater.

Nanocomposite preparation

To fabricate TPO nanocomposite with 3, 5 and 7 wt% nanoclay, a groove with 2mm width was machined in the middle of the base material. The cross-sectional area of processed (Ap) zone was 90 mm² and the density ratio (Dr) was 0.53 (density of nanoclay divided to the density of base material).The dimension of the groove and height of nanoclay particle in the groove was calculated using Eqs. 22-24 as shown in Table 3.

$$Wt(\%) = \frac{A_s}{A_p} \times 100 \qquad (22)$$
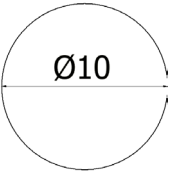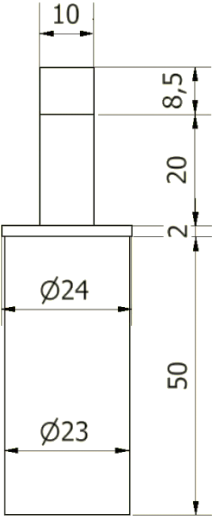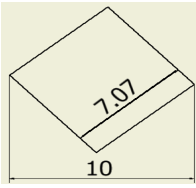
$$h_s = \frac{A_s}{T_s} \qquad (23)$$
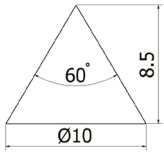
$$h_n = \frac{h_s}{D_r} \qquad (24)$$

In which wt (%) is the weight percent, A_s is the cross-sectional area of groove, T_s is the width of groove, h_n is the height of the nanoclay particle and hs is the height of groove.

Table 1. List of materials and their characteristics.

Material	Company	Grade name	Characteristics
PP	Arak	HP502N	Density = 0.91 g/cm³ and MFI at 230°C, 2.16 kg = 12 g/10 min
EPDM	Petrochemical (Iran)	KEP 270	Mooney viscosity ML (1+8 min) 120°C = 48 M
	Kumho polychem (Korea)		
Nano clay	Southern clay (USA)	Cloisite 15A	(64% ethylene and 8.7% ENB content), Density = 0.82 g/cm³ specific gravity = 1.66 g/cm³

Table 2. Geometry and dimension of frictions stir tools (mm).

	Name	Pin Dimension (mm)	Dimension (mm)	Tool shape
1	Plain and Threaded cylindrical pin	Ø10	10 / 8,5 / 20 / 2 / Ø24 / Ø23 / 50	
2	Square pin	7.07 / 10		
3	Threaded taper pin	60° / 8.5 / Ø10		

The TPO/clay nanocomposites were fabricated by a Deckel milling machine (M.S.T Co, Iran). Nanoclay particles to a height of h_n were compacted into the groove in the middle of the base material. The rotating pin was plunged into the groove until the tool shoulder touched the plate and then the tool was moved along the groove with constant speed for producing the TPO nanocomposite. The FSP parameters, their units and levels are presented in Table 4. The formulation of PP/EPDM/clay nanocomposites used in this study is summarized in Table 5. Figure 2 shows the TPO/5% clay nanocomposite fabricated by the threaded cylindrical pin.

Test procedures
Tensile test of the TPO / clay nanocomposites was carried out at room temperature with a 1 kN load and a cross-head displacement rate of 5 mm/min using a Zuker testing machine. Impact test was performed on notched specimens using a Zwick machine with energy of 1 J. The reported values of responses presented in Table 3 are the average of at least three test measurements. Standard tensile and impact test

specimens as shown in Figure 3 were prepared from the TPO/clay nanocomposites sheets fabricated by FSP according to ASTM standards D638 and D256 [24].

X-ray diffractometer (XRD) was used to evaluate the dispersion of clay in the TPO matrix. XRD experiments were carried out with a Philips -X'Pert diffractometer at room temperature at low angle of 2θ. The X-ray beam was a CuKα radiation (λ = 1.540598 Å) operated at 50 kV voltage and 40 mA current. The scanning rate was 0.25 °/min and the experiments were performed in the angle range of 0 – 10°. TEM observation was performed on ultrathin sections of cryomicrotomed thin nanocomposite films by a Jeol transmission electron microscopy (JEM-2100F) with an acceleration voltage of 100 kV.

Table 4. Process parameters, their units, notifications and levels.

Parameters	Unit	Notification	Level
Rotational speed	rpm	w	1200
Traverse speed	mm/min	S	45
Shoulder temperature	°C	T	125

Table 5. Code and composition of PP/EPDM nanocomposites.

Sample ingredient	S_0	S_1	S_2	S_3
PP	80	80	80	80
EPDM	20	20	20	20
Clay	0	3	5	7

Table 3. Dimension of slot and height of nanoclay particles.

Sample Wt (%)	A_s (mm²)	T_s (mm)	h_s (mm)	h_n (mm)
3% nanoclay	2.7	1	2.7	1.43
5% nanoclay	4.5	2	2.25	1.19
7% nanoclay	6.3	2	3.15	1.67

Theoretical models for prediction of mechanical behaviour of the PP/EPDM nanocomposites fabricated by friction stir process

IPPI

Figure 2. Sample fabricated with threaded cylindrical pin.

RESULTS AND DISCUSSION

Effect of pin geometry on mechanical properties

Table 6 shows the effect of pin geometry on mechanical properties of the TPO/clay nanocomposites fabricated by four different types of tools. According to the results and Figure 4, comparing X-ray diffraction patterns of the samples fabricated by straight cylindrical pin (T_4) and threaded cylindrical pin (T_1) shows that the specimens processed with T_1 tool exhibited lower XRD angle compared to the other tool. When the threaded pin was used, stirring and frictional heat generated by the pin increased and better mixing and dispersion of the nanoclay through the processed zone were obtained by this tool [25]. According to Table 7, comparing the contact surfaces of the three thread pin tools with the base material shows that T_1 tool has a larger contact surface and as a result causes more frictional heat. Consequently, the higher heat generation and better stirring are the reasons for better dispersion of the nanoclay in the base material and obtaining superior mechanical properties [26].

The lower diffraction angle of TPO/clay nanocomposites fabricated by the threaded pin in comparison with those fabricated by the straight pin demonstrates the polymer chains in the specimens fabricated by the former can better intercalate between
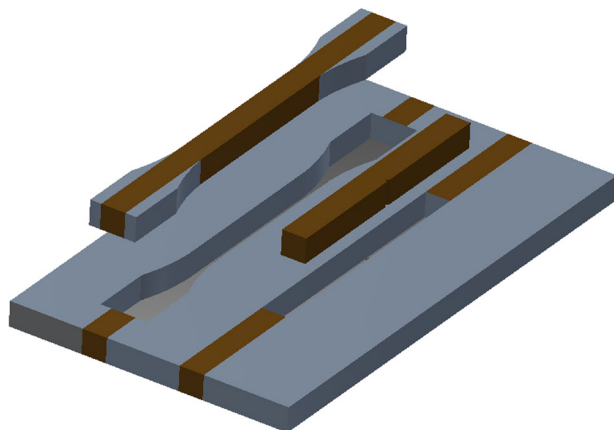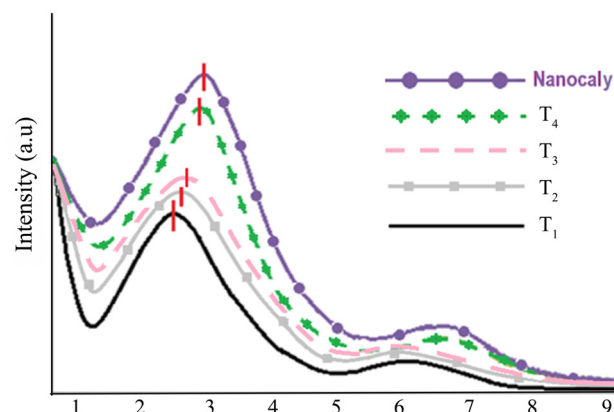

Figure 4. XRD patterns of samples fabricated by different tools.

the layers of the clay, which indicates that the pin shape and geometry can affect XRD diffraction pattern.

The transmission electron microscopy (TEM) micrograph of the PP/EPDM nanocomposite with 3% nanoclay prepared with T_1 tool is shown in Figure 5. The TEM analysis shows that the silicate layer has been dispersed well in the PP/EPDM matrix. It can be observed that a lot of single plates of nanoclay are present in the base material. The TEM micrograph confirms that intercalated and exfoliated morphologies are obtained in this sample.

Effect of nanoclay content on mechanical properties

According to the results in previous section, the tool with threaded pin is better for fabrication of the TPO nanocomposites. The mechanical properties of the TPO nanocomposites having 3, 5 and 7% wt nanoclay fabricated by T_1 tool are shown in Table 8. By increasing the clay content in the matrix the tensile strength and tensile modulus are increased but the impact strength and elongation-at-break are decreased [27, 28]. It is noted that the tensile strength and tensile modulus are, respectively, increased by 44% and 32% with the addition of 7 wt% clay to the PP/EPDM composite. The improvement of tensile strength and tensile modulus of PP/EPDM nanocomposites are related to the reinforcement phenomenon due to the interfacial interaction between the base material and dispersed nanoclay [29]. The X-ray diffraction patterns for different TPO nanocomposite samples are shown in Figure 6. According to these results, the higher dispersion and better intercalation/exfoliation of the clay platelets are observed in the low clay content under the same process parameters condition ($\omega = 1200$ rpm, $S = 45$ mm/min and $T = 125°C$). At the low clay

Figure 3. Scheme of the laser cut of the tensile and Izod specimens from the FSP plates.

Table 6. Mechanical properties of base material and samples fabricated with different tools.

Name	Tensile strength (MPa)	Impact strength (J/m)	Tensile modulus (MPa)	Elongation-at- break (%)
Base material	15.8	87	568.4	146
Threaded cylindrical pin (T$_1$)	21.06	41	709.92	38
Threaded square pin (T$_2$)	19.23	44	673.04	41
Threaded taper pin (T$_3$)	18.79	40	640.65	48
Straight cylindrical pin (T$_4$)	16.4	45	605.73	46

content, polymer chains can intercalate better between the layers of the clay which causes more improvement in tensile strength and tensile modulus [27-29].

Investigation on stress – strain behavior by hyperelastic models

Conventional hyperelastic models such as Mooney – Rivilen, second order polynomial, Neo – Hooken, Yeoh, Arruda – Boyce, Van der Waals and the third- and sixth-order Ogden models were used to predict the stress - strain behavior of PP/EPDM/clay nanocomposites. The ABAQUS software was used to determine the material constant of hyperelastic models utilizing curve fitting and least square fit. The material constants of the hyperelastic models are listed in Tables 9 to Table 11. Figure 7 shows comparison of experimental data with those obtained from the models for PP/EPDM nanocomposite with different nanoclay contents. According to Figure 7 (a), for the PP/EPDM composite, the small difference between the experimental data and the sixth-order Ogden models indicates that the model can predict the results with adequate accuracy. A close inspection of the stress – strain behavior of PP/EPDM composite in Figure 8 (a) shows that at low strain region (0 to 1.5 %), the sixth-order Ogden model has a good agreement with the experimental data, whereas according to Figure 8 (b), at high strain region (8 to 10 %), the third and sixth-order Ogden models show a good agreement with the experimental data. Similar behaviors in the stress – strain curves of nanocomposites materials have been reported by other researchers such as Esmizadeh et al [30-32]. The stress – strain behavior of nanocomposites with 3, 5 and 7 %wt nanoclay shown in Figures 7 (b), (c) and (d), respectively indicates that in these samples the experimental data have a good agreement with the

sixth-order Ogden models. According to the results in Figure 7, for the PP/EPDM composite and PP/EPDM nanocomposites, the theoretical data predicted by Mooney – Rivilen, Neo – Hooken, Yeoh, Arruda – Boyce and Van der Waals show more disagreement with the experimental data in all strain regions.

A micromechanical model for prediction of Young's modulus

Mechanical properties can be improved when a nanoparticle is added to a polymer matrix, although the improvement is usually nonlinear. To predict the Young's modulus of composite and nanocomposites, IROM, LROM and Halpin–Tsai equations have been used by previous researches [33, 34]. According to Figure 9, comparison of the experimental Young's modulus with the results of the mentioned models for the PP/EPDM/clay nanocomposite shows more disagreement between the experimental data and predicted values when clay content increases.

In this study, a quadratic function was used as a modifying factor to predict Young's modulus of the PP/EPDM/clay nanocomposite. The modifying factor

Table 7. Pin surface area for different pin profiled tool.

Name	Threated circular	Threated square	Threated taper
Pin surface area (mm²)	345.4	289.5	266.9
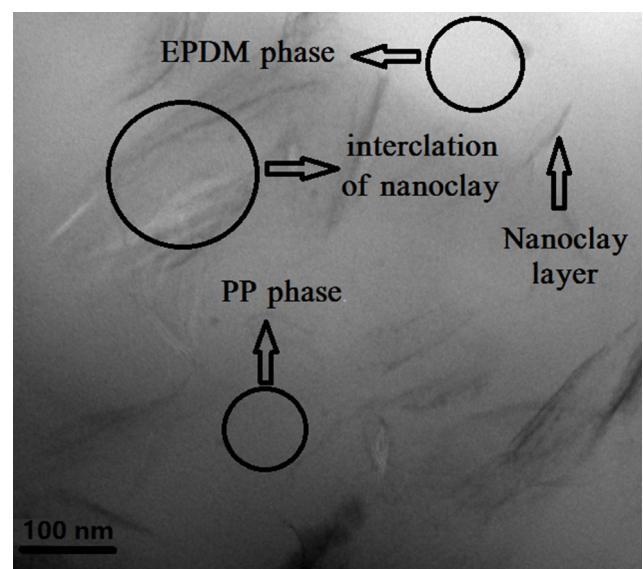
Figure 5. TEM micrograph of PP/EPDM/clay (5%) fabricated by threaded circular tool.

Theoretical models for prediction of mechanical behaviour of the PP/EPDM nanocomposites fabricated by friction stir process

IPPI

Table 8. Mechanical properties of TPO nanocomposites fabricated with threaded cylindrical tool.

| Sample	Tensile strength (MPa)	Impact strength (J/m)	Tensile modulus (MPa)	Elongation-at-break (%)
S_0	15.8	87	568.4	146
S_1	18.94	53	670.80	41
S_2	21.06	41	709.92	38
S_3	22.76	35	751.63	27

is based on the percentage of nanoclay (φf) that is given below:

$$\text{Modifying factor} = a\varphi_f^2 + b\varphi_f + c$$

The final mathematical model, which can be used to predict the Young's modulus of PP/EPDM/clay nanocomposites (E_c), is given in Eq. 26.

$$E_c(\text{Modified model}) = E_c(\text{model}) \times \text{Modifying factor} \qquad (26)$$

The parameters a, b and c are determined by fitting the experimental data with the models. These parameters for the LROM, IROM and Halpin – Tsai models are given in Table 12. The validity of the modified model was checked by comparing the experimental data with the predicted data achieved from the proposed modified
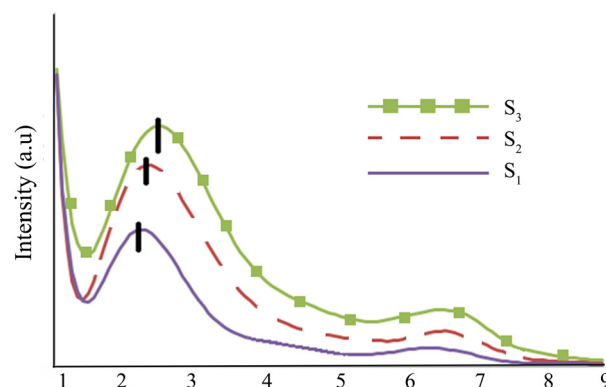
Figure 6. XRD patterns of PP/EPDM nanocomposites fabricated by threaded circular tool.

models. The experimental data, data predicted by conventional models and modified models and mean sum of error are given in Table 13. The small sum of error values between the experimental data and proposed modified models data indicates that these models can predict the Young's modulus with a good approximation.

CONCLUSION

In the present study, the effect of pin geometry

Table 9. Material parameters of the Mooney– Rivlin, polynomial, Yeoh and Neo – Hookean models for PP/EPDM nanocomposite.

Sample code	Mooney - Rivlin		Polynomial (N=2)					Yeoh			Neo - Hookean
	C_{10}	C_{01}	C_{10}	C_{20}	C_{01}	C_{11}	C_{02}	C_{10}	C_{20}	C_{30}	C_{10}
S_0	0.18	4.2	16.5	0.86	-26.2	-3.5	-2.1	1.11	-1.56	1.01	0.45
S_1	0.22	4.7	16.7	1.17	-21.3	-3.7	-3.1	1.3	-1.8	1.1	0.55
S_2	0.24	5.57	17.2	1.32	-19.3	-4.2	-3.7	1.48	-2.07	1.37	0.61
S_3	0.26	6.54	21.6	1.24	-16.2	-4.4	-5.1	1.66	-2.4	1.57	0.67

Table 10. Material parameters of the Arruda - Boyce, Ogden (N=3) and Neo – Van der Waals models for PP/EPDM nanocomposite.

Sample code	Arruda - Boyce			Ogden (N=3)						Van der Waals			
	μ	μ_0	λ_m	μ_1	μ_2	μ_3	α_1	α_2	α_3	μ	λ_m	α	β
S_0	0.90	0.90	56931	496	1.6	-96	0.65	6.8	0.42	2.8	51.9	0.093	0
S_1	1.11	1.11	20.9	460	-185	-251	0.52	0.8	0.5	3.2	51.3	0.095	0
S_2	1.22	1.22	56769	369	-191	-317	0.39	0.8	0.54	3.76	51	0.097	0
S_3	1.33	1.33	56667	141	3.35	-311	0.35	0.6	0.11	4.3	50	0.1	0

Table 11. Material parameters of the Ogden (N=6) models for PP/EPDM nanocomposite.

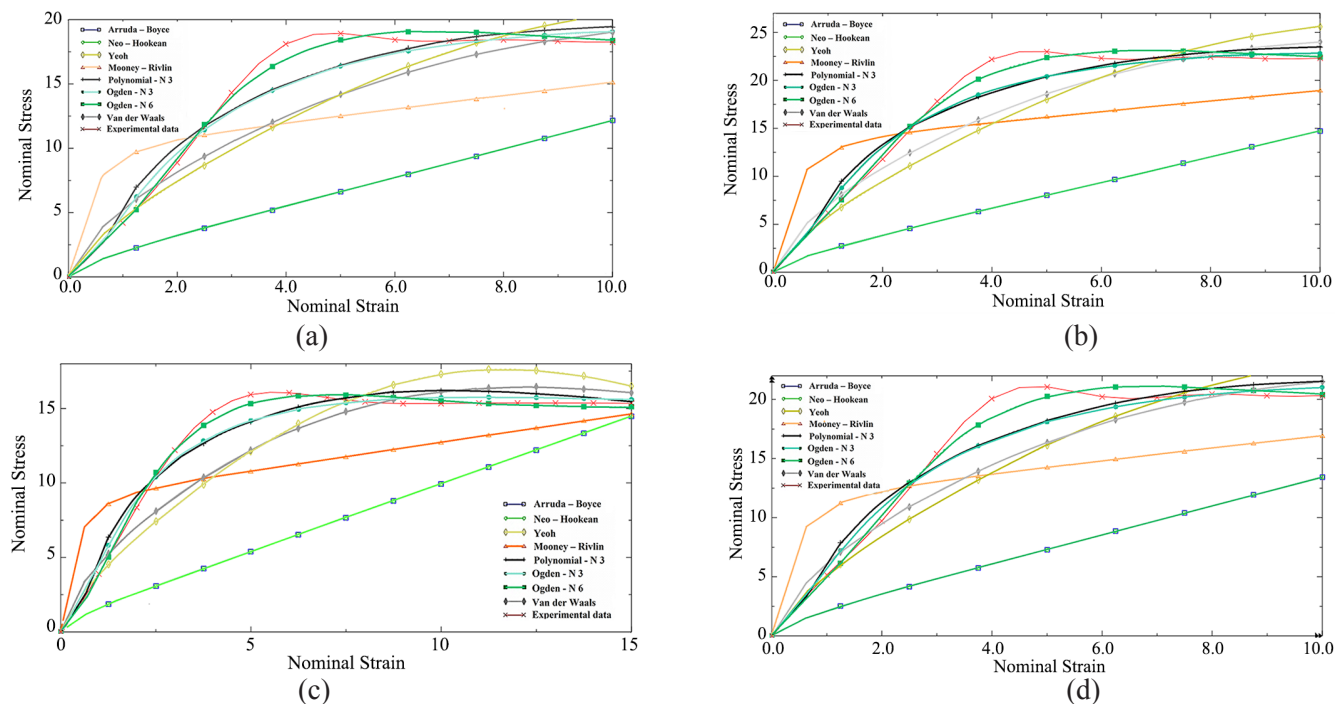| Sample code	Ogden (N=6)											
	μ_1	μ_2	μ_3	μ_4	μ_5	μ_6	α_1	α_2	α_3	α_4	α_5	α_6
S_0	61	-54	-0.14	193	- 211	19	0.26	2.01	3.3	-1.6	-2.4	-4.9
S_1	87	104	-24	-469	668	-354	0.29	2.19	2.7	-1.1	-2.1	-3.9
S_2	104	144	-46	-549	832	-455	0.36	2.24	2.5	-0.6	-1.9	-3.5
S_3	114	97	-55	-664	- 480	- 545	0.39	2.3	2.4	-0.4	-0.5	-3.3

Figure 7. Nominal stress versus nominal strain curves for PP/EPDM nanocomposites (a) S0 , (b) S2, (c) S2, (d) S3.

on the mechanical properties of PP/EPDM/ clay nanocomposites fabricated by FSP has been investigated. PP/EPDM/clay nanocomposites with 3, 5 and 7 %wt nanoclay was produced to investigate the effect of nanoclay content on the mechanical properties and strain – stress behavior of these nanocomposites.

Figure 8. Nominal stress versus nominal strain curves for PP/EPDM nanocomposites in (a) low strain, (b) high strain.

Also a modifying factor depending on clay content was used to improve the theoretical prediction of the Young's modulus of PP/EPDM/clay nanocomposites. It was concluded that:

The mechanical properties and XRD diffraction showed that the threaded pin is better than straight pin for fabrication of polymer nanocomposites.

Tool with higher contact surface with the base material caused more heat generation and stirring in the processed zone, leading to better dispersion of the nanoclay and improvement of the mechanical properties of PP/EPDM/clay nanocomposites.

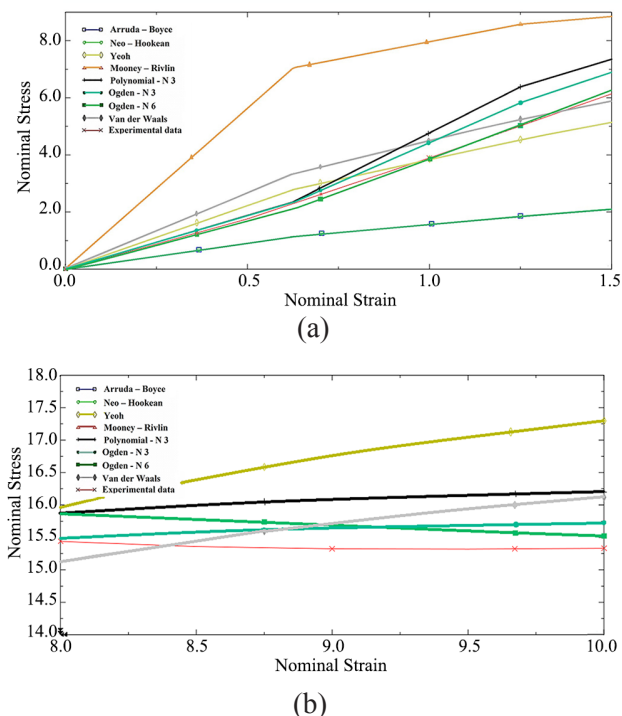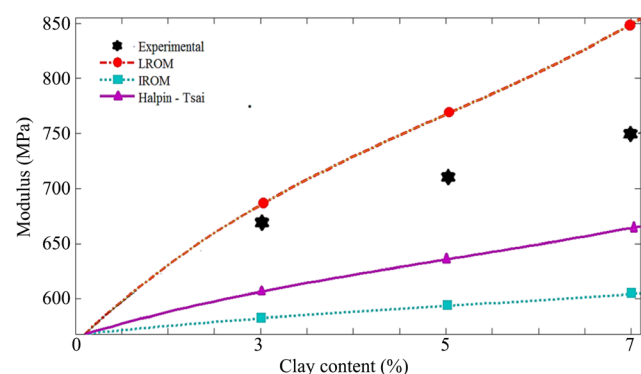Increase in clay content from 0 to 7 wt% increased the tensile strength and tensile modulus and decreased

Figure 9. Comparison of the experimental data and theoretical models for Young's modulus of PP/EPDM nanocomposites.

Theoretical models for prediction of mechanical behaviour of the PP/EPDM nanocomposites fabricated by friction stir process

IPPI

Table 12. Parameters for proposed modifying factor of Halpin- Tsai, LROM and IROM models.

		a	b	c
1	Halpin - Tsai	1.25	0.55	1.083
2	LROM	12.5	-3.5	1.064
3	IROM	12.5	1	1.109

the impact strength and elongation-at-break of these nanocomposites.

The addition of nanoclay had a great effect on the tensile behavior of PP/EPDM/clay nanocomposites. Comparison of hyperelastic models showed that the sixth-order Ogden model had an agreement with stress – strain curve of these composite and nanocomposites.

The conventional models such as LROM, IROM and Halpin – Tsai were limited for prediction of Young's modulus of the nanocomposites. A quadratic function as a modifying factor added to the mentioned models resulted in better prediction of Young's modulus in PP/EPDM/clay nanocomposites.

REFERENCES

1. Taub AI, Krajewski PE, Luo AA, Owens JN (2007) The evolution of technology for materials processing over the last 50 years: The automotive example. JOM 59 (2): 48–57

2. Bahri N, Nekoomanesh M, Sadjadi S, Pajouhan A, (2016) Polyolefin and olefin production in Iran: Current and future capacities, Polyolefins J 3: 11-22

3. Molavi F, Soltani S, Naderi G, Bagheri R, (2016) Effect of multi-walled carbon nanotube on mechanical and rheological properties of silane modified EPDM rubber, Polyolefins J, 3:69-77

4. Naderi G, Lafleur PG, Dubois C (2008) The influence of matrix viscosity and composition on the morphology, rheology, and mechanical properties of thermoplastic elastomer nanocomposites based on EPDM/PP. Polym Compos 29: 1301-1309

5. Nakhaei MR, Mostafa Arab NB, Naderi G (2013) Application of response surface methodology for weld strength prediction in laser welding of polypropylene/clay nanocomposite. Iran Polym J 22: 351-360

6. Hidayah IN, Mariatti M, Ismail H (2015) Evaluation of PP/EPDM nanocomposites filled with SiO_2, TiO_2 and ZnO nanofillers as thermoplastic elastomeric insulators, Plastics. Plast Rubber Compos. 44 (7): 259-264

7. Liu P, Zhong W, Shi H (2009) Polymer-grafted magnetite nanoparticles via a facile in situ solution radical polymerisation. J Exp Nanoscience 4: 323-329

8. Xiangfa Z, Hanning X, Jian F (2012) Preparation, properties and thermal control applications of silica aerogel infiltrated with solid–liquid phase change materials. J Exp Nanoscience 7: 17-26

9. Kiruba VSA, Dakshinamurthy A, Subramanian PS (2015) Green synthesis of biocidal silver-activated charcoal nanocomposite for disinfecting water. J Exp Nanoscience 10: 532-544

10. Sun N, Apelian D (2015) Composite fabrication in cast Al A206 via friction stir processing. Int J Cast Metal Research 28: 72-80

11. Morisada Y, Fujii H, NagaokaFukusumi T.M (2006) MWCNTs/AZ31 surface composites fabricated by friction stir processing. J Mater Sci Eng A 419: 344-348

12. Morisada Y, Fujii H (2008) Nanocomposites fabricated by the friction stir process. Weld inter 22: 15-21

13. Mishra RS, Ma ZY, Charit I (2003) Friction stir welding and processing. Mater Sci Eng A 341: 307-310

14. Elangovan K, Balasubramanian V (2008) Influences of tool pin profile and tool shoulder diameter on the formation of friction stir

Table 13. Young's Modulus of PP/EPDM nanocomposite predicted by different models.

Sample	Experimental data (MPa)	Analytical prediction for different specimens					
		Halpin - Tsai	LROM	IROM	Modified Halpin - Tsai	Modified LROM	Modified IROM
S_0	568.40	568.40	568.40	568.40	568.40	568.40	568.40
S_1	670.80	608.82	690.46	583.60	670.08	669.91	671.28
S_2	709.92	637.15	771.6	594.59	709.54	710.06	708.71
S_3	751.63	666.29	854.24	605.18	751.32	751.94	750.57
Mean Sum of Error		73.03	61.37	116.34	0.47	0.44	0.60

processing zone in AA6061 aluminium alloy. Mater Des 29: 362-373

15. Kumar N, Komarasamy M, Nelaturu P, Tang Z, Liaw PK, Mishra RS (2015) Friction stir processing of a high entropy alloy Al0.1CoCrFeNi. JOM 67: 1007-1013

16. Barmouz M, Seyfi J, Besharati Givi MK, Hejazi I, Davachi S (2011) A novel approach for producing polymer nanocomposites by in-situ dispersion of clay particles via friction stir processing. Mater Sci Eng A 528: 3003-3006

17. Azarsa E, Mostafapour A (2013) On the feasibility of producing polymer–metal composites via novel variant of friction stir processing. J Manuf Process 15: 682-688

18. Zinati F.R. (2015) Experimental evaluation of ultrasonic-assisted friction stir process effect on in situ dispersion of multi-walled carbon nanotubes throughout polyamide 6. Int J Adv Des Manuf Technol 81: 2087-209

19. Marckmann G, Verron E (2006) Comparison of hyperelastic models for rubber-like materials. Rubber Chem Technol 79: 835-858

20. Ali A, Hosseini M, Sahari B (2010) A review and comparison on some rubber elasticity models. J Sci Ind Res 69: 495-500

21. Karimi A, Navidbakhsh M, Beigzadeh B, Faghihi S (2013) Hyperelastic mechanical behavior of rat brain infected by Plasmodium berghei ANKA – Experimental testing and constitutive modeling. Int J Damage Mech 15: 1-15

22. Halpin JC, Kardos JL (1976) The Halpin-Tsai equations: A review. Polym Eng Sci 16: 344-352

23. Kalaitzidou K, Fukushima H, Miyagawa H, Drzal T (2007) Flexural and tensile moduli of polypropylene nanocomposites and comparison of experimental data to Halpin-Tsai and tandon-weng models. Polym Eng Sci 47: 1797-1803

24. ASTM Standard D 638 (1997) Standard test method for tensile properties of plastics In: Annual book of ASTM standard

25. Payganeh GH, Mostafa Arab NB, Dadgar Y, Ghasemi FA, Saeidi Boroujeni M (2011) Effects of friction stir welding process parameters on appearance and strength of polypropylene composite welds. Int J Math Phys Eng Sci 6: 4595-4601

26. Bilici MK, Yukler AI (2012) Effects of welding parameters on friction stir spot welding of high density polyethylene sheets. Mater Des 33: 145-152

27. Naderi G, Khosrokhavar R, Shokoohi S, Bakhshandeh GR,Ghoreishy MHR (2014) Dynamically vulcanized polypropylene/ethylene-propylene diene monomer/organoclay nanocomposites: Effect of mixing sequence on structural, rheological, and mechanical properties. J Vinyl Addit Technol, doi:10.1002/vnl.21432

28. Naderi G, Lafleur PG, Dubois C (2007) Microstructure-properties correlations in dynamically vulcanized nanocomposite thermoplastic elastomers based on PP/EPDM. Polym Eng Sci 47: 207-217

29. Hejazi I, Sharif F, Garmabi H (2011) Effect of material and processing parameters on mechanical properties of polypropylene/ethylene–propylene–diene–monomer/clay nanocomposites. Mater Des 32:3803-3809

30. Esmizadeh E, Naderi G, Barmar M (2014) Effect of organo-clay on properties and mechanical behavior of Fluorosilicone rubber. Fibers Polym 15: 2376-2385

31. Esmizadeh E, Naderi G, Ghoreishy MHR (2013) Modification of theoretical models to predict mechanical behavior of PVC/NBR/organoclay nanocomposites. J Appl Polym Sci 130: 3229-3239

32. Shokoohi S, Naderi G, Kharazmkia M, Ghoreishy MHR (2015) Hyperelastic model analysis of stress-strain behavior in polybutadiene/ethylene-propylene diene terpolymer nanocomposites. J Vinyl Addit Technol, doi:10.1002/vnl.21480

33. Zeng QH, Yu AB, Lu GQ, (2008) Multiscale modeling and simulation of polymer nanocomposites. Prog Polym Sci 33: 191-269

34. Kate KH, Enneti RK, Park SJ, German RM, Atre SV (2014) Predicting powder-polymer mixture properties for PIM design. Crit Rev Solid State Mater Sci 39: 197-214